THE PENNSYLVANIA STATE UNIVERSITY
SCHREYER HONORS COLLEGE

DEPARTMENT OF PHYSICS

Diffractive Dissociative Production of Heavy Vector Mesons in Ultra Peripheral Collisions from LHC to FCC

MICHAEL T. SAYLOR
SPRING 2023

A thesis
submitted in partial fulfillment
of the requirements
for a baccalaureate degree
with honors in Physics

Reviewed and approved* by the following:

Anna M. Staśto
Professor of Physics
Thesis Supervisor

Richard W. Robinett
Professor of Physics
Honors Adviser

*Signatures are on file in the Schreyer Honors College.

Abstract

We investigate the process of the diffractive production of the J/ψ vector meson in the ultra-peripheral proton-lead collisions at LHC and FCC-hh energies. We focus on the diffractive process at large momentum transfer, $-t$, when the proton or a lead nucleus dissociates and its remnants are still separated by the large rapidity gap from the vector meson. The process is directly sensitive to the properties of the Pomeron, a color singlet composite of gluons, which is responsible for the of the presence rapidity gap. The energy and t dependence of the pomeron is described by the solution to the non-forward BFKL equation. The ultraperipheral collisions between protons and lead at LHC allow for a study of this process in a large rapidity range. The rapidity distributions of J/ψ are computed in the case when the Pomeron interacts with the proton as well as in the case when it couples to the nucleus. Predictions for the energies of the FCC hadron-hadron collider are also made.

Table of Contents

List of Figures

List of Tables

Acknowledgements

First, I would like to thank Dr. Anna Staśto for her guidance throughout my work on this thesis. Conducting theoretical physics research using software and data from CERN was something that I would not have believed I would have experienced before graduating with my undergraduate degree. Despite having no experience in conducting this type of research, Dr. Anna Staśto took the time to make sure I understood the research I conducted in addition to allowing me to conduct this research. Despite having her research to complete, she still took the time to help me become a better physicist by pushing me academically beyond what I thought I could do. Her guidance will remain with me throughout my career and is one of the best things I got out of my undergraduate career.

Second, I would like to thank Dr. Richard Robinett for being a wonderful advisor to me. I could always count on him to guide me through my academic career and help me talk through the multiple different academic and career paths that suited my interests.

I also like to thank my family for supporting me throughout my undergraduate career and helping me complete my undergraduate degree in physics with honors. I did not think completing such a task was within my reach, but they proved me wrong through their guidance. The support of my family has allowed me to be as successful as I am which has made me eternally grateful.

Finally, I would like to thank Dr. Anna Staśto and The Eberly College of Science at The Pennsylvania State University for financially supporting me in my research.

Chapter 1

Introduction

1.1 Quantum Chromodynamics and Mesons

Particle physics is the branch of physics that studies the smallest particles of our universe and their interactions. These particles are called elementary particles. At these sizes, a quantum description must be employed, as the wave-particle duality of quantum particles does not allow classical physics to be an accurate description of their behavior.

Currently, there are four fundamental forces known in nature: gravity, electromagnetism, and weak and strong interaction. Three of these forces, weak, strong, and electromagnetic, have consistent descriptions within the quantum framework. There is still an active debate about the proper description of the gravitational interaction with quantum effects included. The two main candidates for quantum gravity are the M-theory [1] and loop quantum gravity [2]. The quantization of electromagnetism leads to the theory of electrons, positrons, and photons, the latter being the quanta of an electromagnetic field. The weak force, which is present in a very short range, is responsible for some of the radioactive decay, such as β decay, and plays an important role in the nuclear fusion process that occurs in the Sun. The strong nuclear force is what keeps the entire nucleus together since it overcomes the electrostatic repulsion of same-charge protons. Quantum Chromodynamics (QCD) is a quantum field theory, see e.g. [3], which gives the strong nuclear force a more fundamental level, as this theory describes how quarks are bound together through the exchange particle called the gluon. The quarks and gluons are relevant degrees of freedom at very small distance scales.

There are several important properties of QCD. Each quark, which is a fermion, in addition to the fractional electric charge, has a color charge, and this color is confined inside other particles. This means that in the experiment, one can only observe composite particles, consisting of combinations of quarks as well as antiquarks, and these composites are color neutral-known as the confinement property of QCD. The strength of the strong interaction increases with distance, therefore, is very large when quarks are separated at large distance scales and decreases whenever the distance scale is small. The small distance scales can be probed with large energy scales, for example in highly energetic collisions, which can be achieved at modern accelerators like the Large Hadron Collider (LHC). This property of diminishing the strength of interaction at large energy scales is called asymptotic freedom. The other fundamental property of QCD is chiral symmetry breaking, which is related to the phenomenon of the generation of masses of nucleons [4].

Quarks are confined inside a hadron and can have one of three different colors. Baryons and mesons are two of the most common types of hadrons. To a first approximation, at low energies, baryons consist of three quarks, whereas mesons consist of a quark and an antiquark.

In this thesis, the production of J/ψ mesons, a specific type of vector mesons, will be studied in a special process, called diffraction dissociation, in the context of ultraperipheral collisions [5] at the Large Hadron Collider (LHC) and the Future Circular Collider, in a hadron-hadron option, (FCC-hh) [6, 7, 8]. The J/ψ meson comprises a charm and anticharm quark and has a mass of 3096.900 $\pm$ 0.006 MeV [9]. The process studied here will be a production of a J/ψ meson with a very large rapidity gap in an ultra-peripheral proton-lead collision. The J/ψ meson is diffractively produced when a color singlet object, most likely composed of gluons, is exchanged in this process. The main object of interest in this process is this color singlet object, often referred to as the Pomeron.

In the present work, we shall study this process in the so-called ultraperipheral proton-lead

collisions at the Large Hadron Collider and the Future Circular Collider, where one of the incoming particles, in our case a lead nucleus, is the source of the strong electromagnetic field. A noticeable property of the ultra-peripheral hadron-hadron collisions, or UPCs, is that one can study processes that are similar to the processes occurring in the collisions of electrons and hadrons which can be realized in the electron-ion collider. For the particular process studies here, the color singlet object cannot be directly studied using a detector. Instead, the color singlet object is studied indirectly by measuring the J/ψ meson. This method of indirect measurements is possible at sufficiently high energies, which are present at the Large Hadron Collider (LHC) and in the Future Circular Collider (FCC).

1.2 Ultra-Peripheral Collisions (UPCs)

In a traditional collision between two hadrons, the final state produced can be complicated due to hadrons being made of smaller more fundamental particles and the presence of the strong interaction.

Ultra-Peripheral Collisions, UPCs, occur when two hadrons, or ions, interact at very large impact parameters [10] as described in Fig. 1.1. Instead of directly strongly interacting with each other, a cloud of virtual photons surrounding one hadron interacts with the other hadron. These virtual photons are condensed into a disk centered around the source particle when the hadrons travel at relativistic speeds due to the Lorentz contraction factor. These collisions are favored with heavier nuclei since the flux of virtual photons is proportional to Z^2, where Z is the atomic number.

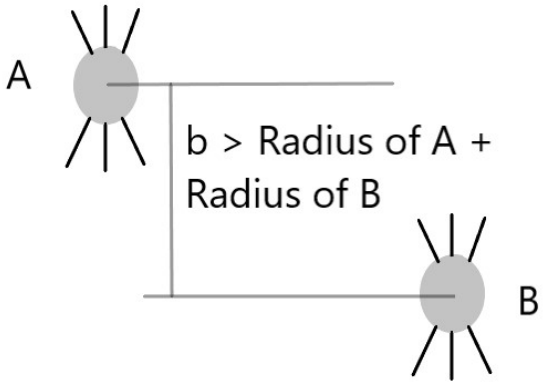

Figure 1.1: This is a diagram of a UPC. The two gray ovals are each hadron traveling at relativistic speeds-hence the distortion along the vertical axis. The lines above and below the ovals describe the electromagnetic fields radiating outwards, creating virtual photons. The gray lines denote the direction of motion of each hadron. The vertical gray line describes the impact parameter, b, which is the distance between each particle and must be greater than the sum of the radius of each hadron for an ultraperipheral collision to occur instead of a traditional collision.

The main benefit to using UPCs is that these types of processes allow for cleaner final states due to the presence of the virtual photons in the interaction, and are very similar to the electron-proton, or ion, collisions. The selection of UPCs allows for the suppression of the direct strong interaction between the hadrons, as they are too far apart from each other [11]. Since the LHC has a very large center-of-mass energy of collisions, these photon-hadron collisions can be studied at energies that are currently not achievable at electron-ion collisions. Of particular interest is the study of diffractive events that are characterized by the presence of large rapidity gaps.

1.3 Diffractive Production of Vector Mesons in UPCs

In this thesis, the diffractive dissociative production of heavy vector mesons, more specifically the J/ψ meson, is studied in the ultra-peripheral collisions of protons with lead nuclei.

The vector meson V is diffractively produced at high energies when a photon γ and a proton p interact with each other, producing a vector meson and the dissociated proton remnant X

$$\gamma + p \to X + V \ . \tag{1.1}$$

The basic Feynman diagram corresponding to the reaction studied is shown in Fig. 1.2. Here, the ultraperipheral collision occurs, since the nucleus, A, is a source of the virtual photon, indicated by the single wavy line.

The 4-momentum of the emitted photon is q^μ, and the virtuality of the photon is therefore

$$q^\mu q_\mu = q^2 = -Q^2 \leq 0 \ . \tag{1.2}$$

The incoming proton has a 4-momentum, P^μ, with the square which is equal to the mass of the proton squared

$$P^\mu P_\mu = P^2 = M_P^2 \ . \tag{1.3}$$

The photon-proton center-of-mass collision energy squared, W^2, is defined as

$$W^2 = (P + q)^2 \ , \tag{1.4}$$

with P and q defined above.

The square of the momentum transfer at the proton vertex, t, a Lorentz invariant, is approximated to be the square of the transverse momentum of the J/ψ meson, $\mathbf{p}_V$,

$$t \approx -\mathbf{p}_V^2 \ . \tag{1.5}$$

The final important Lorentz invariant is the Bjorken, x_{bj},

$$x_{bj} = \frac{Q^2}{2P \cdot q} \tag{1.6}$$

with P and q defined above.

Since the virtuality of this photon is very small (at least compared to any other relevant scales in the problem) we can treat this photon as quasi-real, and assume that $Q^2 = -q^2 \simeq 0$. This photon then interacts with the proton, through the exchange of the color singlet object, the pomeron,

indicated by the gluons in the Feynmann diagram. The vector meson J/ψ is produced due to the interaction of the photon with the pomeron. The Pomeron is an object that has been introduced in the 1960's to describe the behavior of the total cross sections. It has been characterized as the exchange of the quasi-particle with the same quantum number of the vacuum. It was introduced before the QCD became the theory of strong interactions. With the advent of QCD it was necessary to understand as to what is Pomeron in terms of the fundamental degrees of freedom of the theory, and how it couples to other particles. The first pomeron model was independently proposed by Low [12] and Nussinov [13], and in the lowest order it consisted of two gluons. One needs at least two gluons for the color single configuration. Later on a systematic calculation of the gluon exchanges which lead to the dominant behavior at high energy was performed by Balitsky, Kuraev, Fadin and Lipatov [14, 15]. The result is the famous BFKL evolution equation, which sums up all the gluon exchanges that are dominant at very high energy. The solution to this equation gives the gluonic amplitude, which increases like a power with the energy. It is this behavior that is ultimately responsible for the high-energy behavior of the cross section.

In this work, we shall use the solution to the nonforward BFKL equation to calculate the cross section for the diffractive vector meson production at UPCs. The diffractive process means that there is a large rapidity gap between the vector meson produced and the remnants of the proton, p, indicated by the final state X. The rapidity gap is defined as the region in the detector void of any particles. Thus, the gap can be created only if there is color singlet exchange, which corresponds to the Pomeron. The diffractive dissociation means that the rapidity gap is present, but the proton breaks up into a final state X. This process is dominant whenever the momentum transfer at the proton vertex is large. For small momentum transfers the dominant process is the elastic one, i.e. when the proton escapes intact the interaction.

Rapidity is a dimensionless quantity, which is very useful and common for the description of the production of particles in high-energy collisions, see e.g. [16], and is defined by

$$y = \tanh^{-1}\left[\frac{P_z}{E}\right] = \frac{1}{2}\ln\left[\frac{P_z + E}{P_z - E}\right] \ . \tag{1.7}$$

Here, E is the energy of the particle and P_z is the z component of the three-momentum of the particle. The utility of rapidity stems from the fact that it is an additive quantity under Lorentz transformations in the z direction. For very large energies, when the masses of the produced particles can be neglected with respect to their energies and momenta, the rapidity is approximately equal to the pseudo-rapidity, which can be related to the angle θ between the direction of the scattered particles and the direction of the beam. The pseudo-rapidity is defined by

$$\eta = \ln\cot\frac{\theta}{2} \ . \tag{1.8}$$

For massless particles, pseudorapidity and rapidity are identical. For massive particles, they are approximately equal if both particles travel at 0 and 180 degrees with respect to each other in highly energetic collisions.

In this process the object exchanged must be a color singlet. This is essential for the presence of the rapidity gap between the J/ψ and the proton remnant. The purpose of this work is to study this process in UPCs with a photoproduced J/ψ in order to extract properties of the color singlet object-the Pomeron.

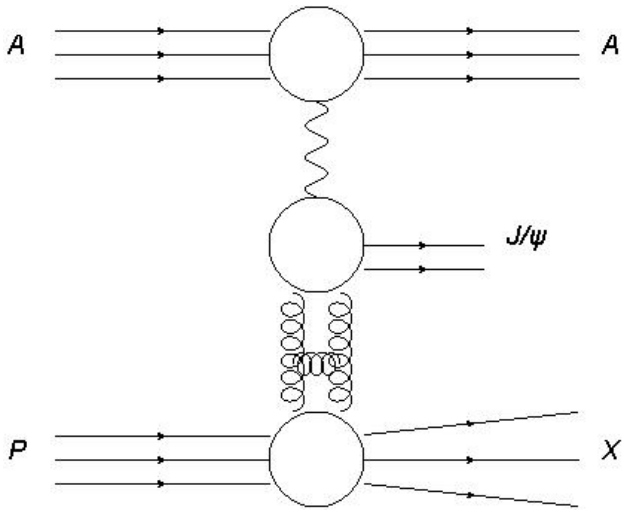

Figure 1.2: This Feynman diagram shows the ultraperipheral collision between a proton, p, and a lead nucleus, A. In this scenario, the proton decays into constituent particles, X, while the lead nucleus remains together. Since this is an ultraperipheral collision, a quasireal photon with $Q^2 = 0$ and a pair of gluons interact with each other to form the J/ψ vector meson. There is a large rapidity gap between the vector meson and the proton remnant X. Here, the cross section of the J/ψ meson is dependent on the product of the photon-proton cross section and the photon flux of the lead nucleus.

Fig. 1.3 shows the Feynman diagram in which the lead nucleus breaks apart into constituent particles, the photon is still interacting with the proton, and the pair of gluons will still interact with the lead nucleus. The photon-nucleus cross section is enhanced by the presence of the nucleus, roughly by a factor A, the mass number. On the other hand, there is a suppression with respect to the previous case, due to the fact that the flux of the photons from the proton is much smaller than the flux of the photons from the lead nucleus. The latter is greater by roughly a factor Z^2, where Z is the atomic number. Overall, the process depicted in Fig. 1.3 has a smaller probability than the process in Fig. 1.2.

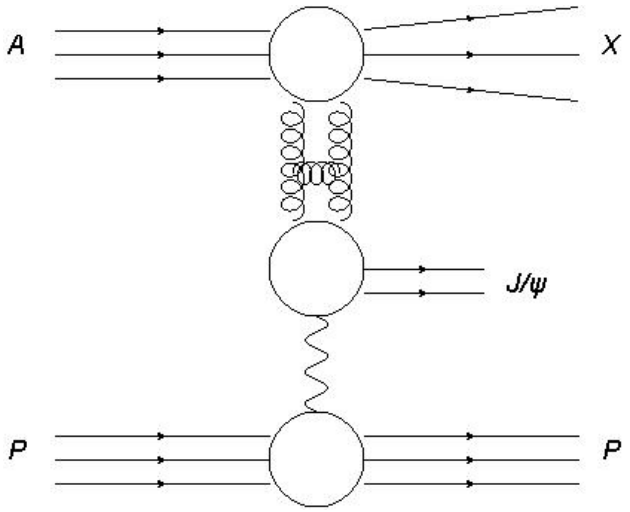

Figure 1.3: This Feynman diagram shows the ultraperipheral collision between a proton, p, and a lead nucleus, A. In this scenario, the lead nucleus decays into constituent particles, X, while the proton remains together. Since this is an ultraperipheral collision, a quasireal photon with $Q^2 = 0$ and a pair of gluons interact with each other to form the J/ψ vector meson. There is a large rapidity gap between the nucleus fragments and the vector meson. Here, the cross section of the J/ψ meson is dependent on the product of the photon-nucleus cross section and the photon flux of the proton.

1.4 LHC and FCC-hh Kinematics

The Large Hadron Collider (LHC) is a high-energy accelerator that performs collisions of protons and nuclei. So far, different combinations of collisions have been studied at the LHC: proton-proton, nucleus-nucleus, and proton-nucleus collisions. Here, we shall focus on the proton-nucleus collisions, where the nucleus is a lead isotope with $Z = 82, A = 208$.

We shall study the collisions of protons with energies of 4 and 7 TeV which can be achieved at the LHC. We shall also study the collisions with higher energy of 50 TeV. This is relevant for the future high energy facility, like the Future Circular Collider hadron-hadron (FCC-hh), which is a next-generation project currently planned at CERN [6, 7]. An FCC collider would have a 50 TeV proton beam and a collision energy of 100 TeV. This thesis includes some of these theoretical calculations. Testing high-energy physics phenomena at higher energy levels is necessary because the theoretical models for quantum particles might not be accurate at higher energy levels-similar to how classical physics is not accurate to describe quantum particles. If these models are not accurate at higher energy levels, then it is possible for theoretical calculations to show some sort of inconsistency with either physical or mathematical logic.

When the calculations are conducted at these higher energies, the energy of the lead nucleus needs to be calculated with

$$E_{Z/N} = E_b \frac{Z}{A} \,, \tag{1.9}$$

where Z is the atomic number 208 and A is the atomic mass 82.

Three different energies were chosen for the calculations are indicated in Table 1.1.

$E_{Z/N}$ (TeV)	E_b (TeV)
19.711	50
2.760	7
1.577	4

Table 1.1: Table of Energies per Nucleon for Lead at Different Energies of a Proton to be used in this thesis.

It is assumed that these very high-energy colliders will have the same engineering as the current colliders in how the collisions are manufactured and detected. In the current colliders, there is a central beam in which the two particles, in this research a proton and a lead nucleus, will be brought to the desired energy and have opposite velocities. Surrounding the central beam near the site of the collision is the cylindrical shell of the detector. This shell will detect the particles that break apart due to the collision.

In this research, the proton or the lead nucleus denoted either particle A or particle B, that breaks apart into remnant particles, collectively denoted X, will be deflected, and the J/ψ meson will travel in the opposite direction due to the conservation of momentum. The J/ψ meson will decay into a pair of electron-positron or pair of muons that will have a curved motion due to the magnetic field within the beam detector that is used to increase the velocity, and consequently, its energy, of the proton and the lead nucleus to facilitate the UPC.

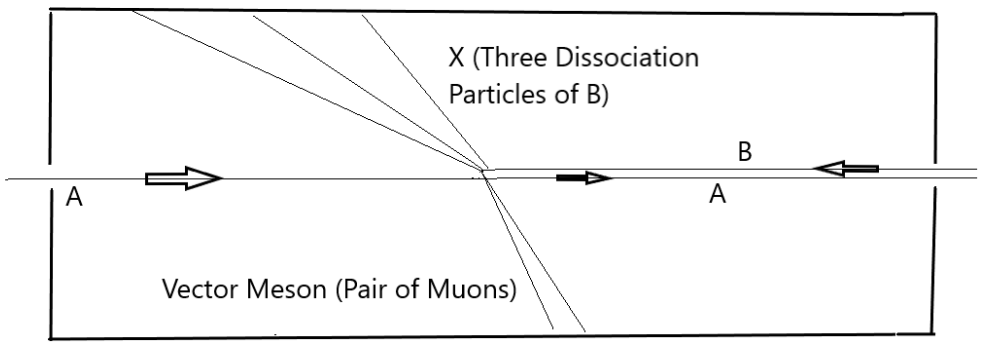

Figure 1.4: This is a side-view drawing of the UPC between particle A and particle B. In this drawing, particle A remains intact after the UPC while particle B dissociates into three particles, collectively denoted X, and travels upward. The J/ψ vector meson, which is a pair of muons, travels downward.

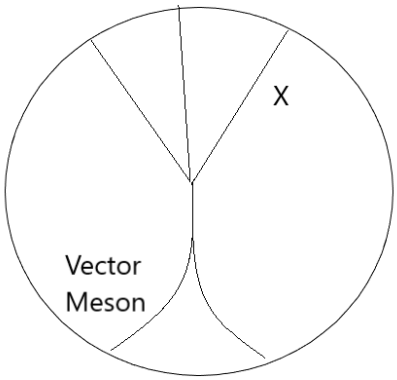

Figure 1.5: This is a cross section drawing of a UPC showing the remnants of one particle, collectively denoted X, and the pair of muons which make up the J/ψ vector meson. The muons travel in a circular direction due to the presence of a strong magnetic field within the beam detector. This drawing shows the theoretical path taken by the particles. In reality, the detector cannot map out all particles with exact precision as there are holes in what the detector can measure. This means the detector would only show part of what is shown in this drawing.

Chapter 2

Theoretical Calculations of Cross Sections and Photon Fluxes

2.1 Introduction

We are interested in the energy and rapidity dependence of the cross section for the J/ψ diffractive production in UPCs in the case when the particle which interacts with the pomeron dissociates, but there is still a rapidity gap between the remnants of the proton, or a nucleus, and the vector meson. This process can be calculated in two steps. First, the emission of the photon from either a proton or a lead nucleus needs to be calculated. This is given by the photon flux, $N_{\gamma/A}(y)$, for a nucleus, and for a proton, $N_{\gamma/p}(y)$. Next, this photon flux needs to be multiplied by the cross section for the production of the J/ψ in a photon-proton or a photon-nucleus collision. In general, the cross section will be given by

$$\frac{d\sigma_{pA\to XAJ/\psi}(y)}{dy} = \sigma_{\gamma p\to J/\psi X}(y) N_{\gamma/A}(y) \ , \tag{2.1}$$

when the photon is emitted from the lead nucleus and the photon then interacts with the proton, which later dissociates as described in Fig. 1.2.

In the reciprocal case, as described in Fig. 1.3, the photon is emitted from the proton and then the photon interacts with the lead nucleus which then dissociates. This cross section is described by

$$\frac{d\sigma_{pA\to pXJ/\psi}(y)}{dy} = \sigma_{\gamma A\to J/\psi X}(y) N_{\gamma/p}(y) \ . \tag{2.2}$$

In Eq. 2.1 and Eq. 2.2, $N_{\gamma/p}(y)$ and $N_{\gamma/A}(y)$ are photon fluxes for the proton and the lead nucleus respectively, and is a dimensionless quantity. The functions $\sigma_{\gamma p\to J/\psi X}(y)$ and $\sigma_{\gamma A\to J/\psi X}(y)$ are the cross sections for the production of the J/ψ in the interaction of the photon with the proton or a lead nucleus respectively. Other variables include: $y = \ln(2\omega/M_{J/\psi})$ is the J/ψ rapidity, ω is the photon energy, and $M_{J/\psi}$ is the mass of the vector meson J/ψ. As we shall see, the photon flux from protons is much smaller than from the nucleus, so in practice the cross section in Eq. 2.2 will be much larger than the cross section in Eq. 2.1.

For the calculations presented in this thesis, we have used the photon fluxes calculated by Guzey and Zhalov in [17]. In that paper, the photon fluxes are calculated from a UPC between a proton and a lead nucleus. The calculation for the cross section for the diffractive vector meson production in dissociation is based on results presented in [18] and used in the thesis [19]. The results in these papers were obtained in the context of the photo-production in an electron-proton collision, and could be adapted in a straightforward way to the case of the ultra peripheral hadron-hadron collisions with quasi-real photons—which is the goal of this thesis.

2.2 Photon Flux in Proton-Pb UPCs

There are many calculations in the literature for the photon flux of a very fast charged particle; see, for example, [20]. Depending on the relative sizes of the particles, such as proton-proton vs. proton-nucleus, there are different approximations that are typically utilized. In this section, we briefly review some of the approaches, following the paper [17], and then in the next chapter we shall show explicit numerical results for the photon fluxes for proton and nucleus in proton-nucleus collisions.

The usual expression for the photon flux of the fast-moving particle with the charge Z is given by

$$N_{\gamma/Z}(\omega) = \frac{2Z^2\alpha_{em}}{\pi^2}\int_0^\infty \left(\frac{F_Z(k_\perp^2+\omega^2/\gamma_L^2)}{k_\perp^2+\omega^2/\gamma_L^2}\right)^2 k_\perp^3 dk_\perp \ , \tag{2.3}$$

where α_{em} is the fine structure constant, γ_L is the Lorentz factor and ω is the energy of the emitted photon. The charge form factor for the particle with charge Z is given by

$$F_Z(Q^2), \ \text{ with the limit of } Q^2 = 0 \text{ being } \ F_Z(0) = 1 \ . \tag{2.4}$$

For the case of the proton, the form factor that is usually used is that of the dipole and can be explicitly defined as

$$F_p(Q^2) = \frac{1}{(1+Q^2/(0.71\text{GeV}^2))^2} \ . \tag{2.5}$$

In that case, when using Eq. 2.5 in Eq. 2.4, we can perform the integral exactly. However, one can approximate the result, which is used for the photon fluxes of the proton in proton-proton UPCs

$$N_{\gamma/p}(\omega) = \frac{\alpha_{em}}{2\pi}\left[1+(1-\frac{2\omega}{\sqrt{s_{NN}}})\right]\left[\ln D - \frac{11}{6} + \frac{3}{D} - \frac{3}{2D^2} + \frac{1}{3D^3}\right] \ . \tag{2.6}$$

In Eq. 2.6, the expressions in the denominators are defined as

$$D = 1 + 0.71\text{GeV}^2\frac{\gamma_L^2}{\omega^2} \ , \tag{2.7}$$

and s_{NN} is the center-of-mass energy squared of the proton-proton interaction.

In the case of the proton-Pb UPC, there is a suppression effect because of the strong interaction between a proton and a lead nucleus that needs to be taken into account. In that case, the photon flux of the fast proton, or a nucleus, is given by

$$N_{\gamma/Z}(\omega) = \int_0^\infty \Gamma_{pA}(\mathbf{b}) N_{\gamma/Z}(\omega,\mathbf{b})\, d^2\mathbf{b} \ . \tag{2.8}$$

Here, the photon flux of the photon from either the lead nucleus or a fast proton is the integral of the photon flux from a distance **b**, called the impact parameter, and is a two-dimensional vector, from the lead nucleus or fast proton, $N_{\gamma/Z}(\omega,\mathbf{b})$, multiplied by the probability of suppressing the strong proton-nucleus interaction, $\Gamma_{pA}(b)$, for small values of the impact parameter **b**.

The photon flux $N_{\gamma/Z}(\omega,\mathbf{b})$ at a transverse distance away from the proton, or a nucleus, is given by Eq. 2.9, where $J_1(bk_\perp)$ is the Bessel function of the first kind and F_Z is the charge form factor of the fast proton or lead nucleus. Since photons radiate outward from their source, the photon flux is dependent on the distance away from its source, which in this case is defined as the impact parameter b. The total flux found in Eq. 2.8 is then integrated over all distances to find the total photon flux, as shown in

$$N_{\gamma/Z}(\omega,b) = \frac{Z^2\alpha_{em}}{\pi^2}\left(\int_0^\infty \frac{k_\perp^2 F_Z(k_\perp^2+\omega^2/\gamma_L^2)}{k_\perp^2+\omega^2/\gamma_L^2} J_1(bk_\perp)\, dk_\perp\right)^2 \ . \tag{2.9}$$

Finally, the probability of suppressing the proton-nucleus strong interaction is given by

$$\Gamma_{pA}(\mathbf{b}) = \exp\left(-\sigma_{NN}\int_{-\infty}^{\infty}\rho_A(z,\mathbf{b})\,dz\right)\ , \tag{2.10}$$

which depends on several inputs. One of them is the total nucleon-nucleon cross section at the corresponding center-of-mass energy, s_{NN}. For the calculations relevant to the LHC energies, σ_{NN} is set to 90 millibarns. When conducting calculations for FCC energies, the same σ_{NN} of 90 millibarns is used. The second input is the nuclear density, $\rho_A(z,b)$.

There are two other approximations that are also used in the literature. One of them neglects the effects of nuclear suppression by setting $\Gamma_{pA}(\mathbf{b}) = 1$, and then sets the lower limit of integration over $d^2\mathbf{b}$ equal to some $b_{\min}$.

The second approximation, very often used in the literature partly due to no integration being used, is given analytically by

$$N_{\gamma/z}(\omega) = \frac{2Z^2\alpha_{em}}{\pi}\left[\zeta K_0(\zeta)K_1(\zeta) - \frac{\zeta^2}{2}(K_1^2(\zeta) - K_0^2(\zeta))\right]\ , \tag{2.11}$$

where K_0 and K_1 are modified Bessel functions of the second kind, $\zeta = \omega b_{min}/\gamma_L$, and b_{min} is a parameter related to the nuclear radius that can be adjusted to reproduce more exact calculations.

Although these approximations are common for calculating the photon flux of the proton, the form factor of a proton is defined analytically by Eq. 2.5, Eq. 2.11 can be used to calculate the photon flux of the lead nucleus when using the form factor data of a lead nucleus from CERN's publicly accessible data.

2.3 $\sigma^{\gamma^* p\to J/\psi X}$ Cross Section

In this section, we shall present the relevant framework for the calculation of the photon-proton cross section to J/ψ and final state X that appears in Eq. 2.1 and Eq. 2.2. This framework for diffractive dissociative production was developed in Refs. [21, 22, 23, 24, 25] and also [26].

To calculate the cross section for the diffractive production of the vector meson in photon-proton collision, one needs to compute the partonic cross section, $\hat{\sigma}_{\gamma^* i}(\hat{s},t)$, for the scattering of the photon on a parton labeled by i. This partonic cross section depends on the center of mass energy between the parton and the photon, $\hat{s}$, and on the momentum transfer, t, which is responsible for the transverse distribution of the produced vector meson.

Next, to calculate the photon-proton cross section, one must sum over all partons in the proton. This is done by multiplication of the partonic cross section with the parton density function (PDF), $f_i(x,\mu)$, for the corresponding parton of species i.

Partons are referred to as the constituent elementary particles that compose a proton or neutron. Quarks and gluons are the partons, but the parton name is still used when a proton is being accelerated and then breaks apart into its constituent particles. Here, the parton densities only include information about the longitudinal momentum fraction of the proton. There exist more complicated parton distribution functions, which contain information about the transverse momentum and spin. The PDF function $f_i(x,\mu)$ can be therefore interpreted as the probability of finding parton i with a longitudinal momentum fraction x of the proton. The PDF also depends on the hard

scale μ, specified below. The final formula for the photon-proton cross section includes summation over all parton species and the integral over the longitudinal momentum fraction x reads

$$d\sigma_{\gamma^* p} = \sum_{i=q,\bar{q},g} \int f_i(x,\mu) d\hat{\sigma}_{\gamma^* i}(\hat{s},t)\, dx \ . \tag{2.12}$$

In the calculations, one needs to specify the scale, μ, of the PDF. For the process in question, we shall choose the typical transverse scale which is given by $\mu^2 = -t + M_V^2$, where M_V is the mass of the heavy vector meson. The photon-parton center-of-mass energy squared $\hat{s}$ can be related to the photon-hadron center-of-mass energy squared W^2 by $\hat{s} \simeq xW^2$, since x is the fraction of the longitudinal momentum of the hadron carried by the parton.

The cross section for the photon-parton interaction is defined in

$$d\hat{\sigma}_{\gamma i}(\hat{s},t) = \frac{C_{\gamma i}}{16\pi \hat{s}^2} |A(\hat{s},t)|^2 \frac{d^2\mathbf{p}_V}{\pi} \ , \tag{2.13}$$

where $C_{\gamma i}$ are the color factors for the scattering of different partons, $\mathbf{p}_V$ is the two-dimensional transverse momentum of the outgoing vector meson, and $A(\hat{s},t)$ is the amplitude for the production of the vector meson.

It is known that at high energies, the imaginary part of the amplitude for this process dominates. It is given by [23, 24]

$$\mathrm{Im}\, A(\hat{s},t) = \hat{s} \int \frac{d^2\mathbf{k}}{2\pi} \frac{\Phi_V(\mathbf{k},\mathbf{p}_V)\Phi_q(\Delta Y,\mathbf{k},\mathbf{p}_V)}{(k^2+s_0)((p_V-k)^2+s_0)} \ , \tag{2.14}$$

where $\mathbf{k}$ is the transverse two-momentum of the exchanged gluon, ΔY is the rapidity gap between the outgoing vector meson and the colliding parton with the longitudinal momentum fraction x, Φ_V is the impact parameter of the vector meson, Φ_q describes the Pomeron and its coupling to the parton.

The formulae above can be used for the case of the Deep Inelastic Scattering of electrons on protons when the photon has virtuality $-Q^2 < 0$, but also in the case of the photo-production when the photon is quasi-real $Q^2 \sim 0$. Therefore, we have used the label γ^* in the formulae of Eq. 2.12 and Eq. 2.13. In UPCs, the photons are quasi-real as indicated by the label γ in Eq. 2.1 and Eq. 2.2.

These cross sections can then be used to calculate the cross section of the produced J/ψ Meson in UPCs. Namely, using Eq. 2.1, the cross section for the photon-proton should be multiplied by the photon flux of the nucleus, which corresponds to the process in Fig. 1.2.

The calculation can also be easily extended to the case represented in Fig. 1.3. In this case, the photon flux from protons should be multiplied by the cross section of the photon on a nucleus. The framework presented above for calculating the cross section can be easily modified to include the nucleus if the PDF of the lead nucleus is used instead of the PDF of a proton.

For the calculation presented here in UPCs, a code for an electron-proton collision was used [19]. The calculation was modified to integrate over the range of the momentum transfer, t, to produce the results as a function of the rapidity, as well as higher energy.

Chapter 3

Numerical Results of the Photon Fluxes

3.1 Photon Flux of the Proton in Proton-Pb UPCs

First, the photon flux of the proton is calculated, which is the process illustrated by Fig. 1.2. The energy of the proton was chosen to be $4\ \mathrm{TeV}$.

To calculate the photon flux of a proton in a proton-Pb UPC, we must use the form factor function of a proton as defined in Eq. 2.5. This form factor will be used in Eq. 2.3 to obtain the resulting photon flux of the proton, as shown in Fig. 3.1.

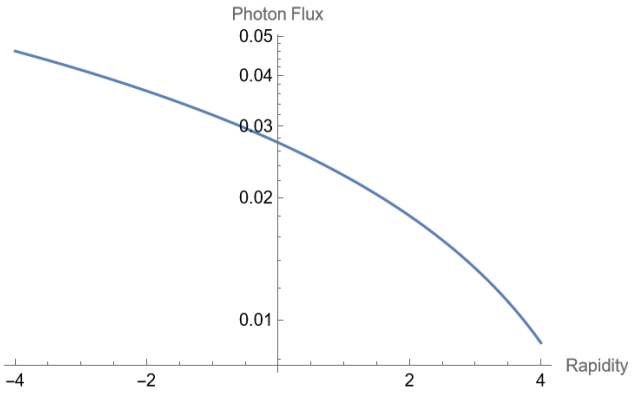

Figure 3.1: Using Eq. 2.3, the photon flux of the proton is calculated in a proton-Pb UPC using the explicit form factor of the proton as defined in Eq. 2.5.

To verify our results, we will use Eq. 2.6 to verify the accuracy of our graph as in Eq. 2.6 is an approximated version of Eq. 2.3. As shown in Fig. 3.4, this approximation is within the same order of magnitude, with only a slight variation in the final result. Eq. 2.6 is favored over Eq. 2.3 as Eq. 2.6 uses a sum of leading terms instead of an integral.

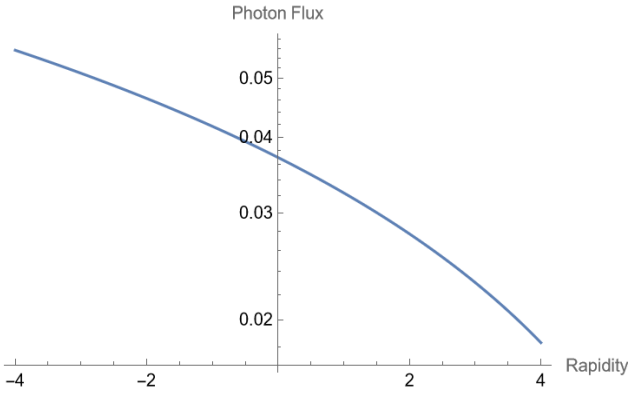

Figure 3.2: Eq. 2.6 is used to verify the photon flux of a proton in a proton-Pb UPC. The similar graphs between Fig. 3.1 and Fig. 3.2 show that the approximated equation for the photon flux of the proton can be used instead of the more exact equation.

3.2 Photon Flux of Pb in Proton-Pb UPCs

Next, we will calculate the photon flux of the lead nucleus in a proton-Pb UPC using three different equations. The fluxes were calculated for the energy per nucleon equal to $1.58\,\mathrm{TeV}$, see Table 1.1. This UPC is illustrated by Fig. 1.3. When calculating the photon flux of a lead nucleus in a UPC between a proton and a lead nucleus, the equations needed become more complicated than multiplying by the atomic number. Instead, different form factor functions must also be used. First, Eq. 2.3 is used to calculate the photon flux of the proton in a proton-Pb UPC. Here, the form factor of the proton is the interpolation of the proton data that was used in [17].

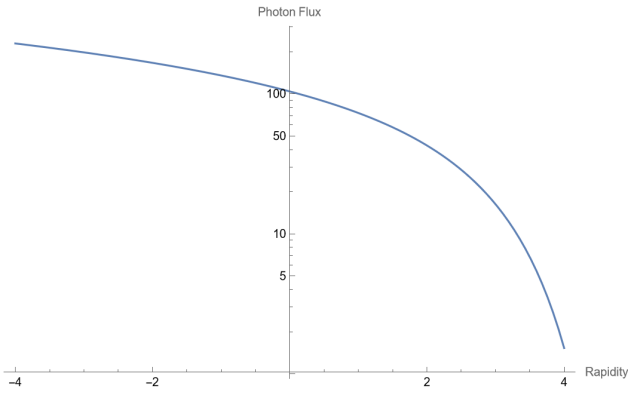

Figure 3.3: Here, Eq. 2.3 is used to calculate the photon flux of the lead nucleus in a proton-Pb UPC.

To verify the accuracy of Fig. 3.3, Eq. 2.8 is used to calculate the photon flux of the lead nucleus in a proton-Pb UPC; however, here, Eq. 2.10 is set to 1. Since Eq. 2.8 is dependent on the range of values of the impact parameter, b, different ranges are used to show its dependence on the resulting photon flux. The oscillations for very small values of the photon flux are proven in 3.3 to be a result of the numerical integration methods used and are not physical phenomena.

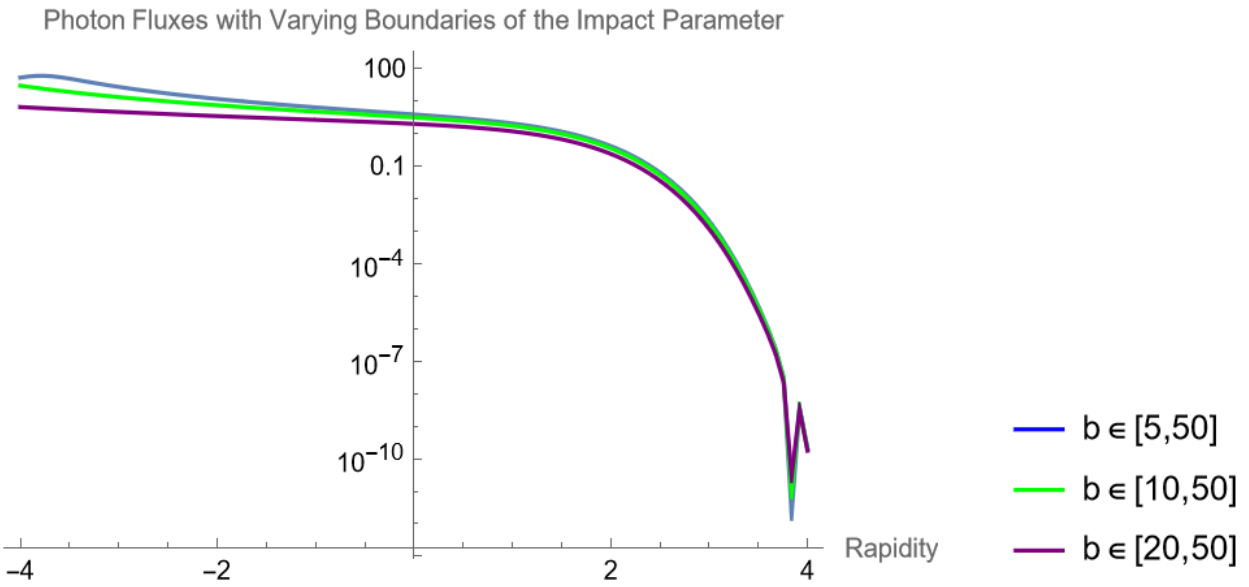

Figure 3.4: When using Eq. 2.8 to calculate the photon flux of a lead nucleus in a proton-Pb UPC, the range of integration of the impact parameter, b, affects the resulting photon flux. The smaller the lower bound of integration of the impact parameter is, the larger the photon flux is for negative rapidity. However, the bigger the lower bound of integration is for the impact parameter, the larger the photon flux is for positive rapidity. Here, the upper bound of integration of the impact parameter is constant at 50 since the photon flux has a greater effect on smaller impact parameters than on larger impact parameters. Any photon flux below 10^{-7} can reasonably be approximated to be 0.

Similarly to calculating the photon flux of a proton in a proton-Pb UPC, we can use a sum instead of an integral to get an approximated result of the graph of photon flux as a function of rapidity, with a major difference being the use of modified Bessel functions of the second kind in our approximated equation, as shown in Eq. 2.11. The resulting graph in Fig. 3.5 shows that this approximation for the photon flux of a lead nucleus is reasonable as the result is the same order of magnitude as Fig. 3.3.

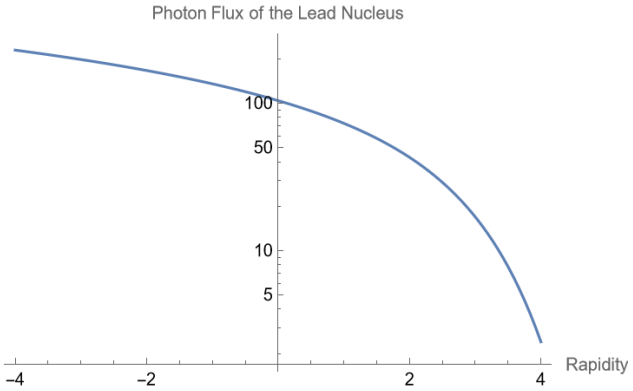

Figure 3.5: Here, Eq. 2.11 is used to calculate the photon flux of a lead nucleus in a proton-Pb UPC.

3.3 Accuracy of Calculated Photon Fluxes

With the small data files used and the need to graph the results, Mathematica was used to calculate the photon fluxes. The equations used needed the use of the NIntegrate function of Mathematica, which approximates the integrals using numerical analysis. This is useful to solve an equation that cannot be explicitly solved; however, there is a potential of introducing errors from the numerical analysis.

To prove that the oscillatory behavior of the photon flux graphs at high rapidity for the UPCs between two protons is a result of Mathematica's calculations instead of the experimental data, we used Eq. 2.8 with a Z value of 1 and using Eq. 2.5 for the form factor of a proton. Fig. 3.7 has oscillatory behavior at large rapidity; therefore, this oscillatory behavior is a result of Mathematica's calculations since we did not use any experimental data in this graph.

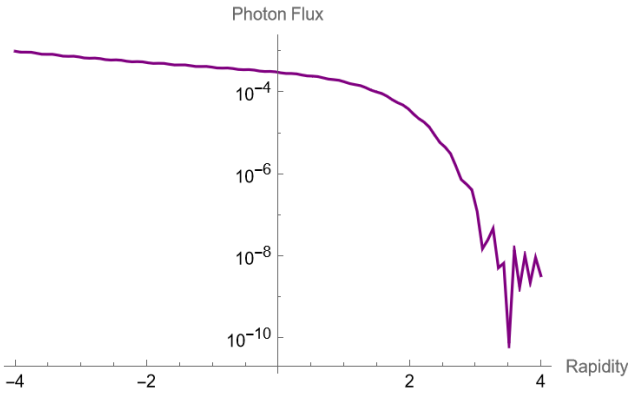

Figure 3.6: Here, the photon flux of a proton wih 1.58 TeV of energy was calculated using only equations and not any data files from an experiment. Since there is still an oscillatory behavior at high rapidity, this behavior must be a result of Mathematica's numerical analysis techniques of NIntegrate instead of a physical phenomenon found within the data files. These oscillations are mostly due to the small values of the photon flux and can be reasonably be approximated to 0.

It is important to know whether or not these oscillatory behaviors are due to experimental data or a result of the numerical approximations used by Mathematica when calculating numerical integrals. In general, the photon flux is inversely proportional to the rapidity. If there were oscillatory behavior due to the experimental data, then there might be an unknown physical phenomenon causing this behavior. Instead, it is just an approximation of the integration of a Bessel function, which itself is an oscillatory function.

Since these oscillations happen for very small values for the photon flux, it is a reasonable approximation to delete the data values below some sufficient value such as 10^{-7}. This oscillatory behavior was also present in Fig. 3.4. Both graphs have oscillations for only the highest positive values for rapidity due to the very small values of the photon flux.

Chapter 4

Numerical Results of the Cross Sections

4.1 Calculating Cross Sections for the Proton and Lead

After adding a loop to integrate the cross section over time and to loop over multiple values of rapidity, the altered code was used to calculate the cross sections of both the proton and the lead nucleus using the CT14nlo and the nCTEQ15_ 208_ 82 parton distribution sets, respectively.

Since the cross sections are larger in magnitude for smaller values for $|t|$, we studied sensitivity to different cutoffs at low t. To visualize the effect that different cutoff values of $|t|$ have on the cross sections, Figure 4.1 shows how using a cutoff of $1\,\mathrm{GeV}^2$ for $|t|$ changes the data with respect to having the lower bound of $|t|$ equal to $0.1\,\mathrm{GeV}^2$ when calculating the cross section. Figure 4.2 shows the effect that different $|t|$ values have when calculating the cross section of the lead nucleus that has an energy of 4 TeV. Notice that in both curves, having a smaller $|t|$ cutoff value corresponded to having a larger cross section for positive rapidities.

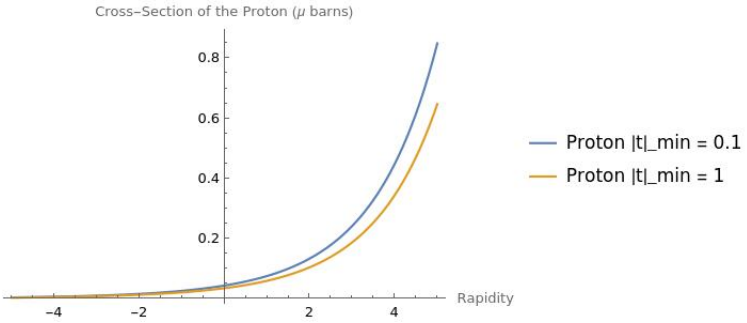

Figure 4.1: Here, the cross section of a proton was calculated using cutoff on $|t|$ equal to $1\,\mathrm{GeV}^2$ (yellow curve) and $0.1\,\mathrm{GeV}^2$ (blue curve) with both having an energy of 4 TeV.

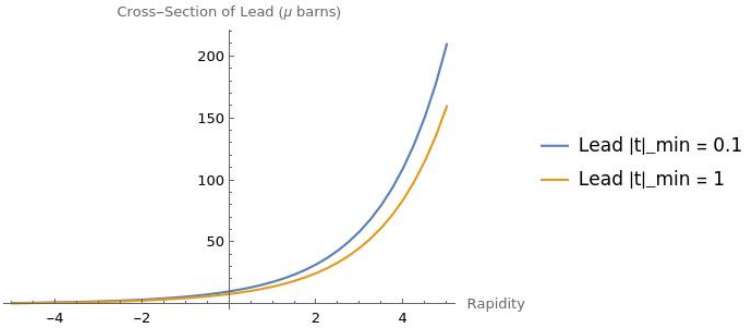

Figure 4.2: Here, the cross section of a lead nucleus was calculated using cutoff on $|t|$ equal to $1\,\mathrm{GeV}^2$ (yellow curve) and $0.1\,\mathrm{GeV}^2$ (blue curve) with both having an energy of 4 TeV. Since the nCTEQ15_208_82 PDF gives the normalized density per nucleon, the cross section of the lead nucleus must be multiplied by $A = 208$.

When calculating the cross section of the proton, the code originally used the CT14nlo PDF data. To see if newer data had a noticeable effect on the resulting cross section, we calculated the cross section using both the CT14nlo PDF data and the newer CT18NLO PDF data. As shown in Figure 4.3, there is no noticeable change in the cross section of the proton when using either the CT14nlo PDF data or the CT18NLO PDF data.

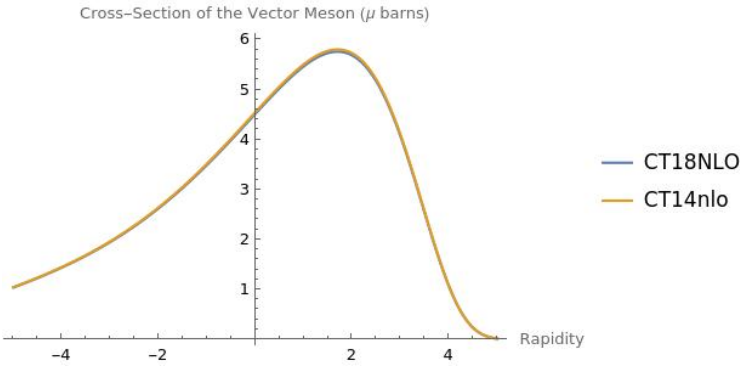

Figure 4.3: The cross section of a proton with 4 TeV of energy as a function of raipdity was calculated using the CT14nlo PDF data (yellow curve) and the CT18NLO PDF data (blue curve). Since there was no noticeable difference in the calculated cross section of the proton, we continued to use the CT14nlo PDF data.

The cross sections of the lead nucleus and the proton, using the nCTEQ15_208_82 and the CT14nlo PDFs respectively, were calculated using the energies described in Table 1.1 and are shown in Fig. 4.4 and Fig. 4.5.

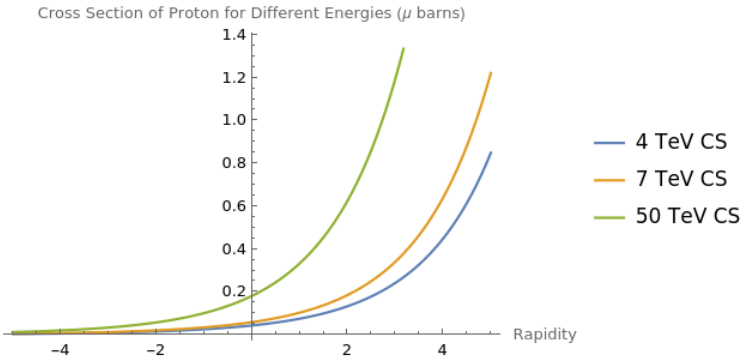

Figure 4.4: The cross section of a proton was calculated using 4, 7, and 50 TeV of energy.

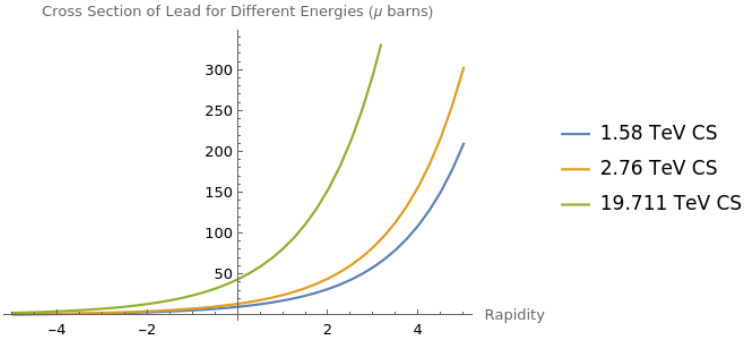

Figure 4.5: The cross section of a lead nucleus was calculated using 1.58, 2.79, and 19.711 TeV of energy. Since the nCTEQ_208_82 PDF gives the cross section per nucleon, the resulting cross section was multiplied by the atomic number of lead, 208.

4.2 Cross Section of the J/ψ meson

From using equation Eq. 2.1, the cross section of the photo-produced J/ψ meson is calculated as the product between the photon flux of the lead nucleus and the cross section of the proton. The other process, Eq. 2.2 is the product of the photon flux of the proton and the cross section of the lead nucleus. Since there are three different energies, there are three different calculated cross sections of the J/ψ vector meson. First, the cross section of the proton will be calculated and then multiplied by the photon flux of the lead nucleus as calculated in Eq. 2.1. This process is illustrated by Fig. 1.2. The cross section as a function of rapidity for this process is shown in Fig. 4.6. At first, we used a constant energy for the particle that generates the photon flux and changed the energy of the particle that dissociates. This is illustrated in Fig. 4.6 through Fig. 4.9.

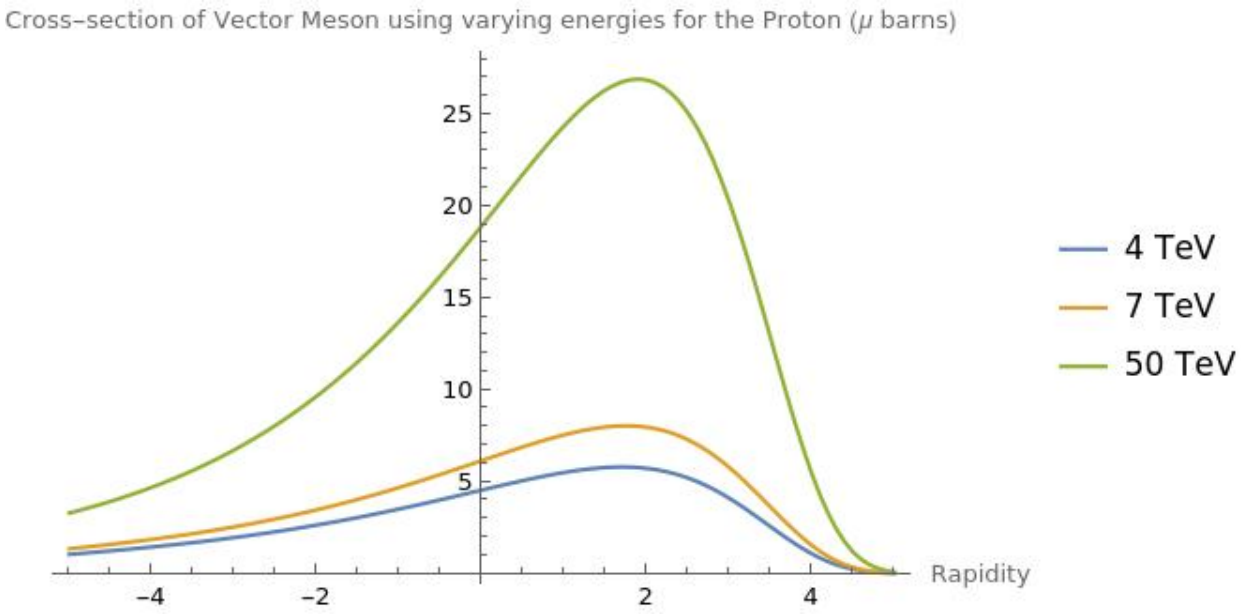

Figure 4.6: Here, the cross section of a J/ψ meson was calculated using Eq. 2.1, in which the cross section of the proton was multiplied by the photon flux of the lead nucleus since the proton dissociates. Here, the photon flux of the lead nucleus is kept constant at 1.58 TeV.

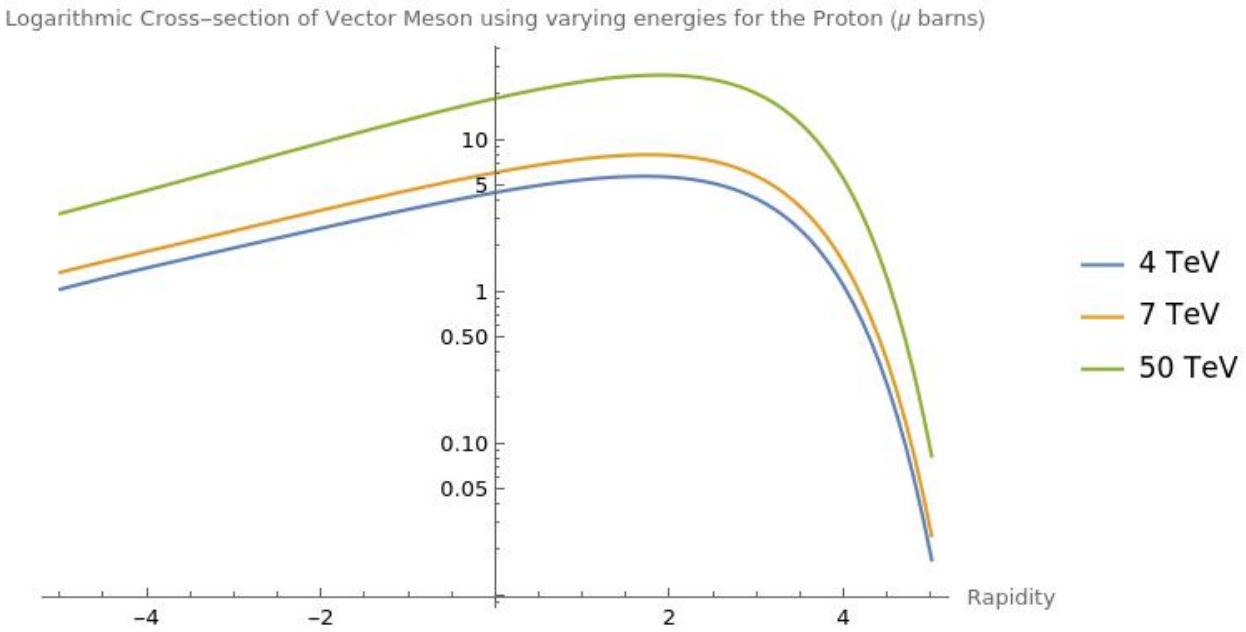

Figure 4.7: Here, the same graph as Fig. 4.6 is shown but in a logarithmic scale.

For the process illustrated in Fig. 1.3 the cross section of the J/ψ meson will be calculated from the cross section of the lead nucleus being multiplied by the photon flux of the proton, as in Eq. 2.2. Similar to previous calculations for the cross section of the lead nucleus, a factor of 208 must be multiplied when using the nCTEQ_208_82 PDF. Here, the photon flux of the proton was calculated using Eq. 2.8 and setting Eq. 2.10 to 1.

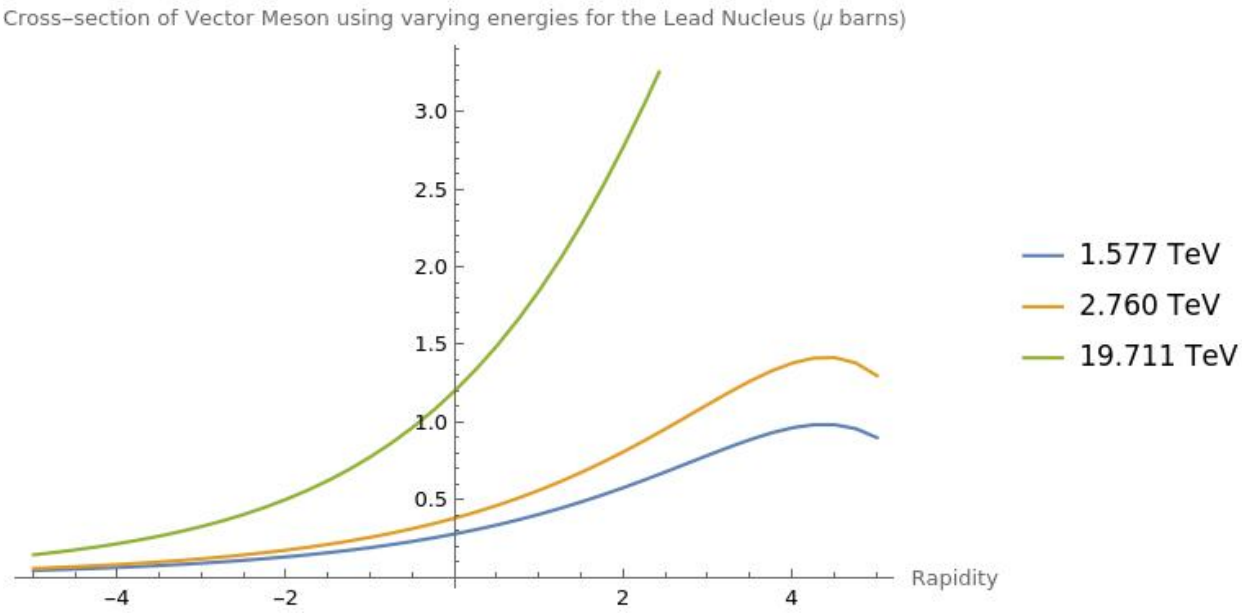

Figure 4.8: Here, the cross section of a J/ψ meson was calculated using Eq. 2.2, in which the cross section of the lead nucleus was multiplied by the photon flux of the proton since the lead nucleus dissociates. Note that the green curve does curve back down, as shown in Fig. 4.7, and the scale used makes it appear to go to infinity. Here, the energy of the proton which generates the photon flux is kept constant at 1.577 TeV.

The cross section of the J/ψ meson production changes appreciably when the energy is increased. This is evident both from Fig. 4.8 and Fig. 4.6. However, the cross section for a production on lead is still smaller than the cross section on the proton. This is evident when looking at the energies per nucleon rather than looking at the total energy of the particle.

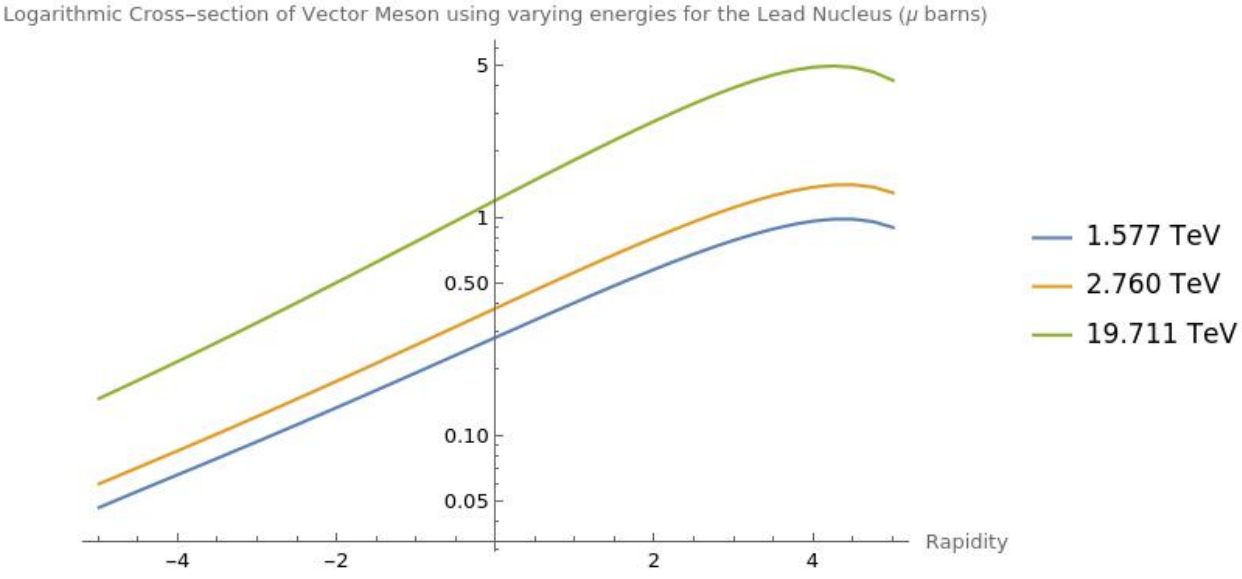

Figure 4.9: Here, the same graph as Fig. 4.8 is shown but in a logarithmic scale.

Next, we calculated the cross section of the J/ψ meson using different energies for the photon flux of the lead nucleus. This setup represents better the type of beam configurations that are possible at the LHC and will be possible at the FCC-hh machine. That is the proton-lead collisions are taken to occur at following pairs $(E_p, E_A/N)$ of energies (in TeV) : $(4 \text{ and } 1.58), (7 \text{ and } 2.76)$ for LHC and $(50 \text{ and } 19.7)$ for FCC.

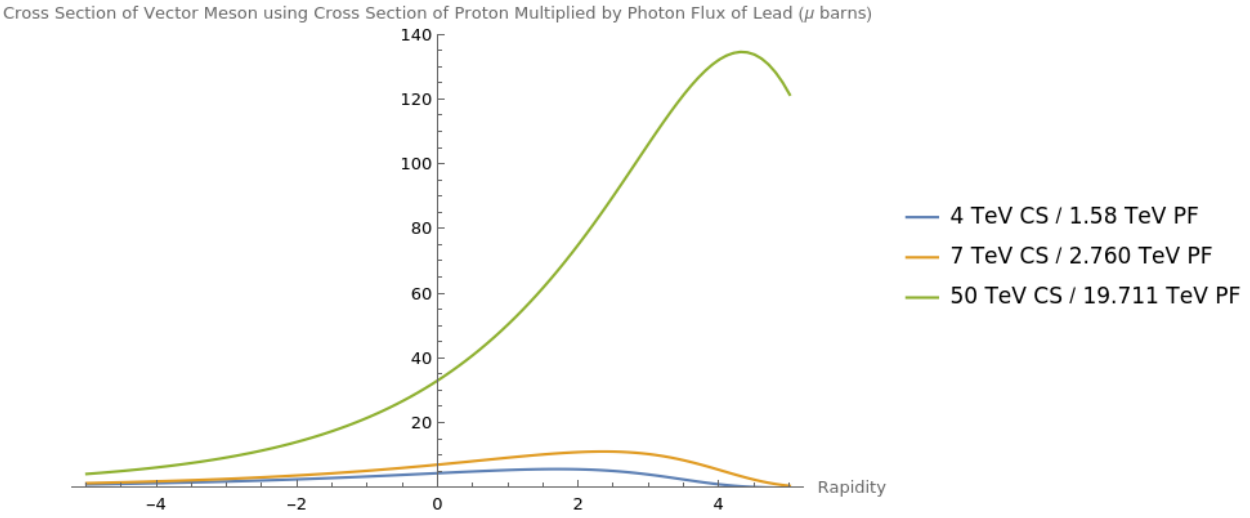

Figure 4.10: Here, the cross section of the J/ψ meson is calculated using different energies for the photon flux of the lead nucleus. We used 4, 7, and 50 TeV for the energies entering the calculation of the cross section of the proton and we used 1.58, 2.76, and 19.711 TeV for the energies of the photon flux of the lead nucleus.

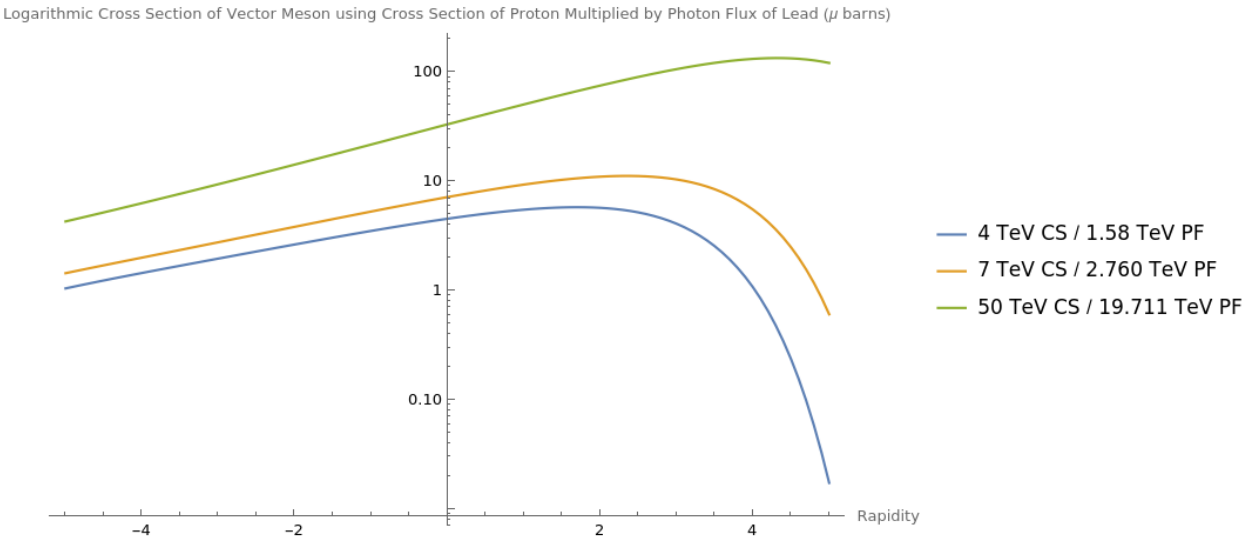

Figure 4.11: Here, the same graph as Fig. 4.10 is shown but in a logarithmic scale.

Finally, we calculated the cross section of the J/ψ meson from Eq.2.2 using different energies for the photon flux of the proton.

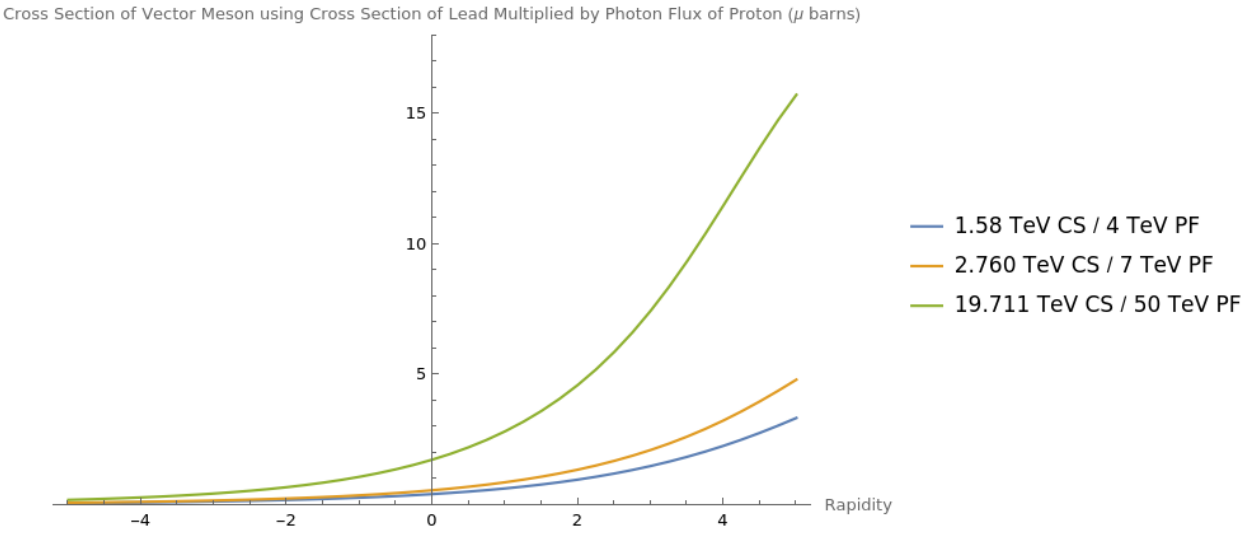

Figure 4.12: Here, the cross section of the J/ψ meson is calculated using different energies for the photon flux of the proton. We used 4, 7, and 50 TeV for the energies of the photon flux of the proton and we used 1.58, 2.76, and 19.711 TeV for the energies of the cross section of the lead nucleus.

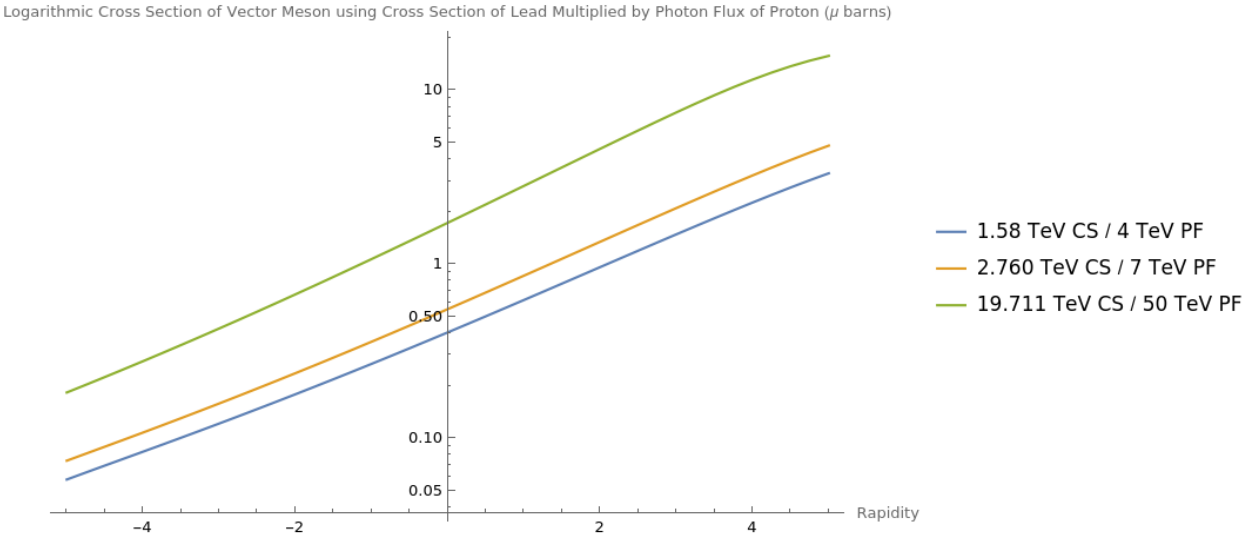

Figure 4.13: Here, the same graph as Fig. 4.12 is shown but in a logarithmic scale.

For the cross section of the J/ψ meson, the peak value shifts depending on whether the proton or the lead nucleus dissociates. The photon flux from the proton has a shallower slope than the photon flux from the nucleus, due different energies per nucleon. As the cross section of the proton and the lead nucleus are both comparable to each other, when normalized, it is therefore the photon flux that has the greater affect on the cross section of the J/ψ meson. Since the photon flux of the proton has a shallower slope, it results in a shift of the peak of the cross section of the J/ψ meson for higher rapidities. This is shown by the maximum value of the J/ψ meson is at a higher rapidity when the lead nucleus dissociates and the photon flux of the proton is multiplied by the

cross section of the lead nucleus compared to when the proton dissociates and the cross section of the J/ψ meson is the photon flux of the lead nucleus multiplied by the cross section of the proton.

From Figs. 4.13 and beyond, we observe that when the energy of the particle generated the photon flux is increased, the peak of the distribution fo the J/ψ meson changes even more with rapidity and is pushed to higher values. This is understood from the fact that the more energetic particle will also produce more energetic photons. The flux of the photons will thus be cutoff at higher energies and this in turn will move the distribution of the produced vector mesons to higher rapidities.

4.3 Accuracy of Calculated Cross Sections

Since the cross sections were calculated using a code written in the C++ programming language, the accuracy of the final numbers depends on the computer used. When comparing the numerical calculations from a computer running Ubuntu to a computer running MacOS, the first 8 digits are the same while the remaining digits vary slightly. To have more accurate results, the average of the numerical calculations should be used; however, such precision is not needed in this thesis and therefore no rounding of several calculations is used.

As shown in Fig. 4.3, there is a possibility that different PDF sets will have different resulting cross sections. Although calculating the cross section of the J/ψ meson could be repeated to include different PDF sets, there should not be a significant change in the resulting cross section of the J/ψ as the PDF sets used have high accuracy.

Chapter 5

Conclusion

The diffractive dissociative production of the J/ψ vector meson in ultraperipheral collisions was studied at LHC and FCC-hh energies. This process is mediated by the exchange of the pomeron, a color singlet composite object of gluons responsible for the rapidity gap in this process.

The cross section for the production of vector mesons with rapidity gap was calculated from a convolution of the photon flux and the photon-hadron cross section. The latter one used the solution to the non-forward BFKL equation to describe the pomeron. Both the photon being emitted by the lead nucleus and the photon being emitted by the proton were considered.

We have studied different forms of the photon fluxes which are available in the literature. The photon flux of the lead is much larger than the photon flux from the proton, since it is enhanced by a large factor, roughly being proportional to the square of the atomic number Z. We have checked that the approximated formulae for the photon fluxes give reasonably close results to the more accurate predictions which involve full form factors and integrals over the impact parameter dependence of the photon source.

The cross section for the process in which the proton dissociates was computed by convoluting the photon fluxes from lead and the photon-proton cross section. The results were integrated over the momentum transfer t, and we found that they depend on the lower cutoff used of the momentum transfer as the cross section peaked at low momentum transfers. We have evaluated the rapidity distributions for three different energies of the proton beam, 4, 7, and 50 TeV, collided with lead beam of energy per nucleon 1.58, 2.76 and 19.7 TeV which correspond to the two LHC energy scenarios and the FCC-hh projection. The rapidity distributions widen and increase with energy. This is driven by the rapidity growth of the pomeron and the changes in the photon flux.

Next, we have calculated the process in which the photon is emitted by the proton and then interacts with lead. In this case, the lead nucleus disintegrates, but there is still rapidity gap between the nuclear remnant and the vector meson. In order to calculated that process, the flux of protons was convoluted with the cross section on lead. The nuclear parton densities were used to estimate the photon-lead cross section using the same framework as for the proton. No other rescattering corrections were included. The overall cross section is smaller in this case, as it is, roughly speaking, suppressed by the atomic number Z^2 from the photon flux, and only enhanced by the mass number A from the lead nucleus. In practice, the suppression is much milder due to the more accurate expressions of the photon flux from the lead nucleus.

In summary, the diffractive dissociative production of vector mesons offers a unique opportunity to study the properties of the color singlet pomeron. The ultraperipheral collisions at LHC and at future FCC-hh are ideal to measure and study this reaction at very high energies where large rapidity gaps can be formed.

Bibliography

[1] K. Becker, M. Becker, and J. H. Schwarz. *String theory and M-theory: A modern introduction*. Cambridge University Press, 12 2006.

[2] Abhay Ashtekar and Eugenio Bianchi. A short review of loop quantum gravity. *Rept. Prog. Phys.*, 84(4):042001, 2021.

[3] William Marciano and Heinz Pagels. Quantum chromodynamics. *Physics Reports*, 36(3):137–276, 1978.

[4] Volker Koch. Introduction to chiral symmetry. In *3rd TAPS Workshop on Electromagnetic and Mesonic Probes of Nuclear Matter*, 12 1995.

[5] Nikolai N. Nikolaev and Bronislav G. Zakharov. Pomeron structure function and diffraction dissociation of virtual photons in perturbative QCD. *Zeitschrift für Physik C Particles and Fields*, 53(2):331–345, 1992.

[6] Michael Benedikt, Alain Blondel, Patrick Janot, Michelangelo Mangano, and Frank Zimmermann. Future Circular Colliders succeeding the LHC. *Nature Physics*, 16(4):402–407, 2020.

[7] A. Abada et al. FCC Physics Opportunities: Future Circular Collider Conceptual Design Report Volume 1. *Eur. Phys. J. C*, 79(6):474, 2019.

[8] A. Abada et al. FCC-hh: The Hadron Collider: Future Circular Collider Conceptual Design Report Volume 3. *Eur. Phys. J. ST*, 228(4):755–1107, 2019.

[9] R. L. Workman et al. Review of Particle Physics. *PTEP*, 2022:083C01, 2022.

[10] Spencer Klein and Joakim Nystrand. Ultraperipheral nuclear collisions. *Physics Today*, 70(10):40, Oct 2017.

[11] A J Baltz et al. The Physics of Ultraperipheral Collisions at the LHC. 2007.

[12] F. E. Low. A Model of the Bare Pomeron. *Phys. Rev. D*, 12:163–173, 1975.

[13] S. Nussinov. Colored Quark Version of Some Hadronic Puzzles. *Phys. Rev. Lett.*, 34:1286–1289, 1975.

[14] I. I. Balitsky and L. N. Lipatov. The Pomeranchuk Singularity in Quantum Chromodynamics. *Sov. J. Nucl. Phys.*, 28:822–829, 1978.

[15] E. A. Kuraev, L. N. Lipatov, and Victor S. Fadin. The Pomeranchuk Singularity in Nonabelian Gauge Theories. *Sov. Phys. JETP*, 45:199–204, 1977.

[16] L. Kowalski; L.P. Remsberg; T. Abbott. Rapidity and Invariant Cross Sections.

[17] V. Guzey and M. Zhalov. Rapidity and momentum transfer distributions of coherent J/ψ photoproduction in ultraperipheral pPb collisions at the LHC. *Journal of High Energy Physics*, 2014(2), 2014.

[18] Piotr Kotko, Leszek Motyka, Mariusz Sadzikowski, and Anna M. Staśto. BFKL Pomeron loop contribution in diffractive photoproduction and inclusive hadroproduction of J/ψ and . *Journal of High Energy Physics*, 2019(7), 2019.

[19] Douglas Maxwell Howell. Diffractive Heavy Vector Meson Production at the EIC and LHeC. 2021.

[20] L. Frankfurt, M. Strikman, and M. Zhalov. Large t diffractive J / ψ photoproduction with proton dissociation in ultraperipheral pA collisions at LHC. *Physics Letters, Section B: Nuclear, Elementary Particle and High-Energy Physics*, 670(1):32–36, 2008.

[21] Jeffrey R. Forshaw and M. G. Ryskin. Diffractive vector meson production at large momentum transfer. *Z. Phys. C*, 68:137–148, 1995.

[22] Jeffrey R. Forshaw and G. Poludniowski. Vector meson photoproduction at high t and comparison to HERA data. *Eur. Phys. J. C*, 26:411–415, 2003.

[23] R. Enberg, Jeffrey R. Forshaw, L. Motyka, and G. Poludniowski. Vector meson photoproduction from the BFKL equation. 1. Theory. *JHEP*, 09:008, 2003.

[24] G. G. Poludniowski, R. Enberg, Jeffrey R. Forshaw, and L. Motyka. Vector meson photoproduction from the BFKL equation. 2. Phenomenology. *JHEP*, 12:002, 2003.

[25] Michal Deák, Anna M. Staśto, and Mark Strikman. High —t — diffractive vector meson production at the EIC. *Physical Review D*, 103(1):1–16, 2021.

[26] Halina Abramowicz, Leonid Frankfurt, and Mark Strikman. Interplay of hard and soft physics in small x deep inelastic processes. *eConf*, C940808:033, 1994.

MICHAEL T. SAYLOR

EDUCATION

Bachelor of Science with Honors in Physics Aug 2019 - May 2023
Minors in Mathematics and Nanotechnology The Pennsylvania State University, University Park, PA

EXPERIENCE

Undergraduate Researcher Jan 2022 - May 2023
The Pennsylvania State University, Department of Physics *University Park, PA*

- Calculated high-energy proton-lead UPCs at energies comparable to the LHC and FCC
- Gained programming skills in C++ and numerical analysis skills in Mathematica
- Authored an honors thesis for the Schreyer Honors College

Learning Assistant in Physics Jan 2021 - May 2023
The Pennsylvania State University, Department of Physics *University Park, PA*

- Served as an in-class tutor and took a professional development course
- Helped in both introductory courses with over 200 students and a 400-level course with 25 students
- Nominated and Received an Undergraduate Teaching Excellence Award in 2022

Undergraduate Research Intern June 2022 - Aug 2022
Fermi National Accelerator Lab, Superconducting Quantum Materials and Systems Center *Batavia, IL*

- Research program was administered and funded by Northwestern University and took place at The Fermi National Accelerator Laboratory and had an acceptance rate below 10%
- Authored a research paper after conducting experimental research on the thermal conductivity between copper and niobium at sub-100 millikelvin environments using a dilution refrigerator
- Goal of research was to determine the most thermally efficient materials to be used in the construction of a dilution refrigerator by presenting my work to scientists at The Fermi National Accelerator Laboratory and The National Institute of Standards and Technology

Cohort Student May 2021 - Aug 2021
The Pennsylvania State University, Eberly College of Science *University Park, PA*

- Participated in the Eberly College of Science Research 101 Summer Cohort
- Learned the best practices of conducting undergraduate research both at The Pennsylvania State University and at other institutions through workshops and networking events
- Was chosen as one of 20 out of over 70 applicants and received a scholarship as compensation

LEADERSHIP

- Scholar Ambassador, The Schreyer Honors College
- Volunteer for The Student Farm, The Schreyer Honors College
- Member of the Quantum Information and Computation Club, The Pennsylvania State University
- Treasurer and Youth Volunteer of a religious club, The Pennsylvania State University
- Committee Member for THON, The Pennsylvania State University
- Member of The Society of Physics Students, The Pennsylvania State University
- Grant Chair for Engineers Without Borders, The Pennsylvania State University

NOTABLE COURSEWORK

- I completed a race and criminal justice course which included a trip to Curacao to study the effects of both Dutch Colonization and being a territory of a European country on a Caribbean island
- As a 3^{rd} year undergraduate student, I enrolled in a graduate-level course in quantum information science taught through the Engineering Science department

HONORS AND AWARDS

- 2022-2023 John and Elizabeth Holmes Teas Scholarship Fund, The Eberly College of Science
- 2022 Undergraduate Teaching Excellence, The Pennsylvania State University
- 2021-2022 Elsbach Scholarship in Physics, The Pennsylvania State University
- Dean's List (multiple semesters), The Pennsylvania State University

SKILLS

Technical Skills	Computer programming in C++ and Python, Mathematica, SolidWorks, Technical Writing
Soft Skills	Problem Solving, Communication, Ethical Leadership, Public Speaking, Interpersonal Skills